Velocity-based filtering approach to photoacoustic-guided hysterectomy demonstrated with a human cadaver

Nethra Venkatayogi[a], Karen C. Wang[b], and Muyinatu A. Lediju Bell[a,c,d,e]

[a]Department of Computer Science, Johns Hopkins University, Baltimore, MD
[b]Department of Gynecology and Obstetrics, Johns Hopkins Medicine, Baltimore, MD
[c]Department of Electrical and Computer Engineering, Johns Hopkins University, Baltimore, MD
[d]Department of Biomedical Engineering, Johns Hopkins University, Baltimore, MD
[e]Department of Oncology, Johns Hopkins University School of Medicine, Baltimore, MD

ABSTRACT

Photoacoustic imaging was previously proposed to provide real-time guidance for surgeons to avoid ureteral injury during hysterectomies, by providing photoacoustic-based distance measurements between the surgical tool tip and ureter with photoacoustic-based auditory alerts to warn of dissatisfying proximity. However, acoustic clutter can cause inconsistencies in tool tracking and photoacoustic source information. To address these inconsistencies, we propose a method that leverages the positional information of each photoacoustic source (e.g., tool tip, ureter, uterine artery) along with the velocity of tool movements in lateral and axial directions. By limiting distance measurements based on expected velocities, measured tool locations were confined to a specified region surrounding the tool tip in each frame, constraining the measured tool tip motion within the region boundaries. The acquired photoacoustic frames were synchronized with the corresponding camera footage of the procedure to validate the tool motion. This approach was tested in a 22-frame photoacoustic video of a tool sweep acquired during an operation performed on a cadaver. Calculated velocities in the axial and lateral dimensions were reduced from 8.53±10.12 mm/s and 11.54±14.25 mm/s, respectively, before filtering to 3.45±3.70 mm/s and 3.21±3.86 mm/s, respectively, after filtering. Results demonstrate smoother tool tip tracking with increased robustness to erroneous tool tip detections caused by acoustic clutter, thereby providing more reliable distance measurements and less sporadic auditory information based on these distance measurements. Overall, these results have the potential to improve the effectiveness of a novel velocity-filter-based auditory feedback approach to enhance ureteral safety during hysterectomies.

1. INTRODUCTION

Hysterectomy, the surgical removal of the uterus, requires cauterization and transection of the uterine arteries while avoiding nearby overlapping ureters, which are located within millimeters of the uterine artery.[1] Given the close proximity to the ureter, gynecological procedures correspond to 75% of intraoperative injuries to the ureters.[2] In addition, 50-70% of ureteral injuries are undetected during surgery, leading to increased risks of hospital readmission, additional surgery, prolonged recovery, acute renal insufficiency, sepsis, and death.[3,4] In cases such as endometriosis, pelvic malignancies, or extensive scar tissue from previous surgeries, ureter detection beneath excess tissue is even more challenging due to distorted anatomy.[5,6] These cases can lead to increased incidences of ureteral injury in malignant rather than non-malignant conditions.[4,7]

We previously presented a photoacoustic imaging system to provide real-time guidance for surgeons during hysterectomies to avoid ureteral injury by identifying surgical tool tips, distinguishing the ureter from the uterine artery, and providing photoacoustic-based distance measurements between the surgical tool and the ureter, along with photoacoustic-based auditory alerts to warn surgeons of proximity to the ureter.[8–10] This approach was generally successful with tissue-mimicking phantom studies and open human cadaver experiments.[8,10–12] However, acoustic clutter can cause inconsistencies in tool tracking and photoacoustic source information by obscuring targets of interest and complicating anatomical measurements.[13]

In this work, we address these inconsistencies by introducing a method that leverages the positional information of each photoacoustic source (e.g. tool tip, ureters filled with methylene blue, and uterine artery) along

Photons Plus Ultrasound: Imaging and Sensing 2025, edited by Alexander A. Oraevsky, Lihong V. Wang, Proc. of SPIE Vol. 13319, 133190M · © 2025 SPIE
1605-7422 · doi: 10.1117/12.3044621

with the velocity of tool movements in the lateral and axial photoacoustic image dimensions. In particular, measured tool locations were confined to a specified region surrounding the tool tip in each frame based on expected velocities, constraining the measured tool tip motion within the region boundaries. We test our velocity-based filtering approach on a photoacoustic video of a tool sweep acquired during an operation performed on a cadaver.

2. METHODS

2.1 Experimental setup

An open procedure was performed on a human cadaver. During this procedure, the ureter and distal portion of the uterine artery were dissected and sutured at the distal end. The uterine artery was injected with whole human blood, and the ureter was filled with 400 μM methylene blue mixed with urine. A Phocus Mobile laser (Opotek, Inc., Carlsbad, CA) operating at wavelengths from 690 nm to 800 nm with a pulse repetition frequency of 10 Hz was coupled to a 5 mm-diameter fiber bundle emitting an energy of 31.7 mJ per pulse, respectively. Photoacoustic and ultrasound data were acquired at a rate of 5 Hz per acquisition (due to interleaved alternating data acquisitions per laser pulse). The fiber bundle was fixed with a ring stand. This setup was used to illuminate the ureter and uterine artery. Co-registered ultrasound and photoacoustic data were acquired using an Alpinion ECUBE12R research ultrasound scanner (Alpinion, Seoul, Korea), connected to an Alpinion EC3-10 transvaginal ultrasound probe, with a center frequency of 6 MHz. To provide a comparison for the photoacoustic distance calculation, a video was recorded with an external camera (iPhone 8, Apple, Cupertino, CA) at the same time as the photoacoustic video of the tool motion, with vocal "stop" references used to synchronize the two videos.

2.2 Data Acquisition and Analysis

Ultrasound and photoacoustic channel data were acquired with and without a laparoscopic grasper tool tip (Autosuture Endo Grasp, Medtronic, Fridley, MN) placed in the imaging plane. During the procedure, with the laparoscopic tool in the imaging plane, the tool was navigated between the ureter and uterine artery. First, touching the ureter, then sweeping toward the uterine artery, then touching the uterine artery. This motion was repeated for approximately 6 seconds. These tool sweeps were performed by a board-certified gynecologic surgeon (K.C.W). Co-registered ultrasound and photoacoustic videos of this motion were acquired with the goals of obtaining proximity information and mapping to auditory information.

Delay-and-sum (DAS) beamforming was used to create ultrasound images, while both DAS and short-lag spatial coherence (SLSC)[14,15] beamforming were implemented to create photoacoustic images. Because SLSC beamforming directly displays the coherence of received signals, SLSC images improve visualization compared to DAS images when high-amplitude, incoherent artifacts are present. Therefore, SLSC beamforming was used to identify regions of interest (ROIs) corresponding to the ureter, uterine artery, and the tool. Each DAS or SLSC photoacoustic image was normalized to its brightest pixel prior to display. Photoacoustic images were acquired with 690 nm and 750 nm wavelengths. The 750 nm wavelength was utilized to select the ROIs and calculate distance measurements for all analyses, given the greater contrast difference between the ureter and uterine artery at this wavelength (relative to that achieved with 690 nm wavelength).[9]

The position of tool tip, P_t, and the position of the ureter, P_u, were identified in photoacoustic images created with a single 750 nm laser wavelength, as the tool was navigated between the ureter and uterine artery. In particular, the position of the tool, P_t, was selected as the region surrounding the brightest pixel in the 750 nm image. The region identified as the surgical tool was assigned a green colormap, then temporarily removed from the image (i.e., set to zero). With the tool region removed, the position of the uterine artery was then selected as the region surrounding the brightest pixel in the remaining 750 nm image. This region was assigned to a red colormap, then temporarily removed from the image (i.e., set to zero). With both the surgical tool and uterine artery removed from the image, the position of the ureter, P_u, was then defined as the brightest pixel in the remaining 750 nm image. This region was then set to a blue colormap. The three colormaps (i.e., green, red, and blue) were then combined into a single image. Each identified region was normalized by its brightest pixel and displayed with a dynamic range that enhanced signal visualization.

2.3 Velocity-based filtering

To accomplish velocity-based filtering, a 30-frame photoacoustic video of a tool sweep acquired during an operation, with tool motion validated through the synchronization of the corresponding camera footage, was utilized to create expected velocities. Expected velocities, v_z and v_x, were defined as the maximum possible velocity of the tool motion in the axial and lateral directions, respectively, between each frame in the validated photoacoustic video. The calculated expected velocities were $v_x = 10.68$ mm/s and $v_z = 17.26$ mm/s. Given the expected velocities, the tool tip in a single image frame, T_i, was constrained to a region surrounding T_i defined as $\pm v_x$ and $\pm v_z$ divided by the frame rate. This constrained region was created to confine measured tool locations within the region boundaries. Therefore, the axial, z, and lateral, x, positions of of the tool tip was defined as the brightest pixel in the image based on velocity, $V_i(x, z)$, as follows:

$$T_{\mathrm{i}}(x,z) = \begin{cases} T_{\mathrm{i}}(x,z), & \text{if } |V_i(x)| \le v_x \text{ and } |V_i(z)| \le v_z \\ T_{\mathrm{filter}}(x,z), & \text{Otherwise} \end{cases} \tag{1}$$

where $V_i = (T_i - T_{i-1}) \times$ frame rate, and T_{filter} is the brightest pixel in the constrained region.

The method to calculate tool tip positions using velocity-based filtering described by Eq. (1) was tested in a separate 22-frame photoacoustic video known to have erroneous tool tip detections due to acoustic clutter, as evidenced by the discrepancies in tool motion when compared to the synchonized camera footage. The photoacoustic frames were then synchronized with the corresponding camera footage of the procedure to validate the tool motion, using the vocal "stop" references in the camera video.

3. RESULTS

Figure 1 shows annotated screenshots illustrating photoacoustic target detections in two consecutive frames (i.e., Frame 1 followed by Frame 2). The yellow and green boxes highlight the identified tool locations before and after filtering, respectively. There is an obviously erroneous tool tip detection before filtering, which is resolved with filtering (i.e., the yellow and green box overlap in Frame 1 yet appear at significantly different locations in Frame 2). The significant tool location differences with no filtering are caused by the presence of acoustic clutter artifacts, which are avoided after implementing the proposed velocity filtering approach.

Figure 2(a) shows the axial and lateral tool tip positions and tool-to-ureter distances, before and after filtering. Generally, the tool tip positions in the axial and lateral dimensions follow an expected periodic pattern after filtering (green), when compared to the pattern obtained before filtering (yellow). The resulting tool-to-ureter Euclidean distance was 7.20±3.18 mm before filtering and 4.89±1.17 mm after filtering. To relate these results to

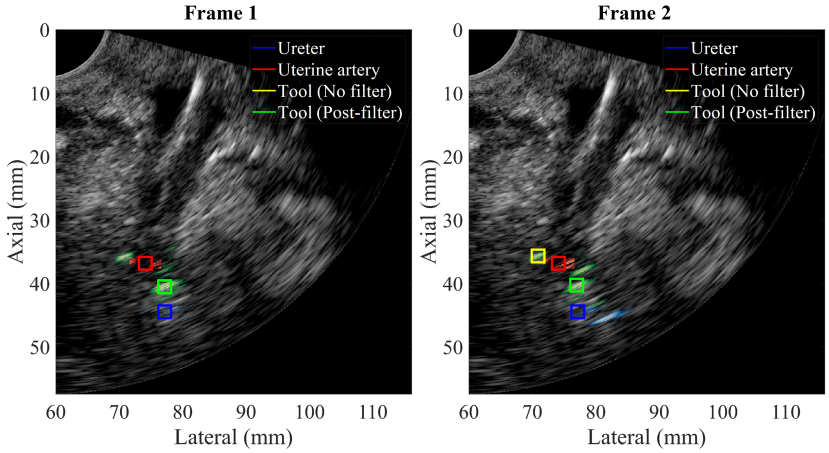

Figure 1. Annotated signals detected in two consecutive frames. There is an overlap between the detected tool tip with no filtering (yellow) and after filtering (green) in Frame 1.

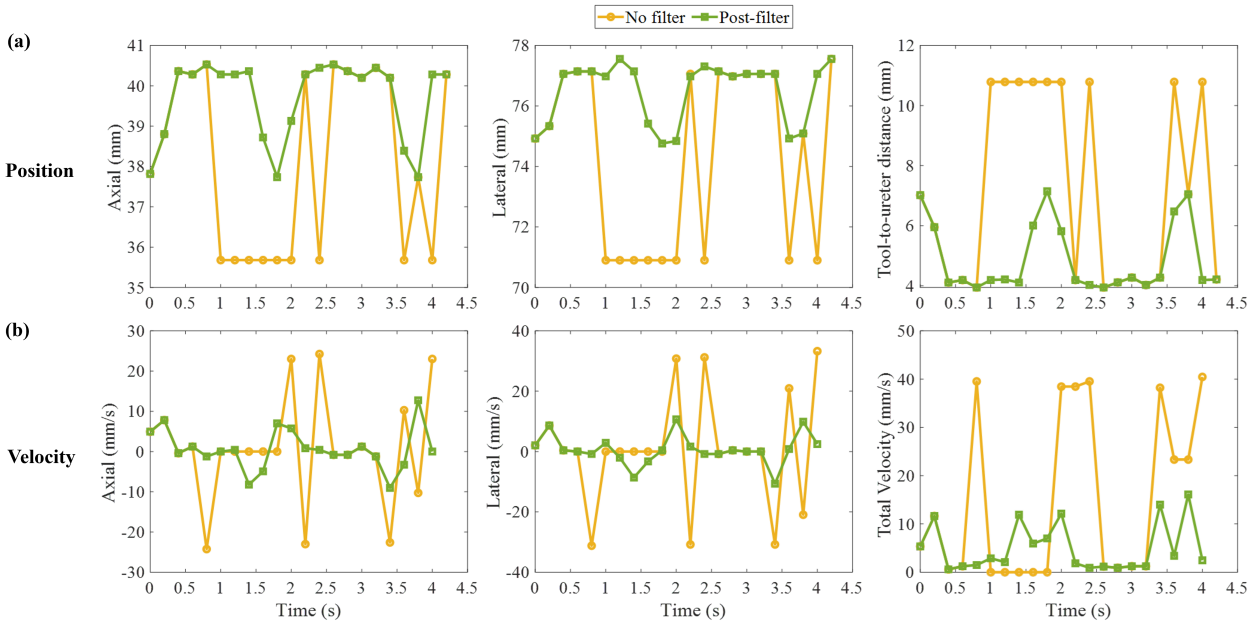

Figure 2. (a) Tool tip positions and distances from the ureter as a function of time. (b) Corresponding axial, lateral, and total tool velocities as a function of time.

the still frames in Figure 1 (which were acquired at timestamps of 0.8 and 1.0 s, respectively), the corresponding decrease at 1.0 s with no filter applied to the calculated tool-to-ureter Euclidean distance reported in Figure 2 is supported by the erroneous tool tip detection in Frame 2. This erroneous detection is corrected at 1.0 s in Figure 2 after filtering is applied.

Figure 2(b) shows the corresponding velocities and total velocities, before and after filtering. The mean ± one standard deviation of absolute values of the velocities in the axial and lateral dimensions were 8.53±10.12 mm/s and 11.54±14.25 mm/s, respectively, before filtering. These values were reduced to 3.45±3.70 mm/s and 3.21±3.86 mm/s, respectively, after filtering. The corresponding total velocity was reduced from 14.51±17.35 mm/s before filtering to 5.02±5.03 mm/s after filtering.

4. DISCUSSION

This work is the first to apply a velocity-based filtering method to address inconsistencies in photoacoustic information and tool tip tracking. The proposed method provides smoother tool tip tracking, as illustrated in Figure 2, and offers increased robustness to erroneous tool tip detections caused by acoustic clutter. As a result, the method allows for more reliable distance measurements, with the Euclidean tool-to-ureter distance decreasing from 7.20±3.18 mm before filtering to 4.89±1.17 mm after filtering, and reduces sporadic auditory feedback, while providing photoacoustic guidance to surgeons during a hysterectomy. The proposed method has the potential to be implemented in other applications of photoacoustic-based surgical guidance systems.[16–20]

Current validation methods for positions and distances calculated from photoacoustic images include synchronization with camera footage and co-registered ultrasound footage. However, this approach lacks ground truth measurements to verify the accuracy of the photoacoustic-based information. Future work will validate calculated positions and distances using a robotic arm to provide absolute tool displacements.

5. CONCLUSION

A velocity-based filtering approach was presented to improve surgical tool tracking, which can be affected by acoustic clutter, to prevent accidental ureteral injuries in photoacoustic-guided hysterectomies. Results demonstrate smoother tool tip tracking, increased robustness to erroneous tool tip detections, and reduced overall

velocities (e.g., 14.51±17.35 mm/s before filtering to 5.02±5.03 mm/s after filtering). The proposed approach is promising to provide more reliable distance measurements and more effective auditory feedback to enhance ureteral safety during hysterectomies (and other procedures that may benefit from similar technology).

ACKNOWLEDGMENTS

This work is supported by NIH R01 EB032358.

REFERENCES

[1] Williams, P., Bannister, L., Berry, M., Collins, P., Dyson, M., and Dussek, J., "Gray's anatomy: the anatomical basis of medicine and surgery," *New York: Churchill Livingstone* **38** (1995).

[2] Chan, J. K., Morrow, J., and Manetta, A., "Prevention of ureteral injuries in gynecologic surgery," *American Journal of Obstetrics and Gynecology* **188**(5), 1273–1277 (2003).

[3] Zaghbib, S., Saadi, A., Boussaffa, H., Ayed, H., and Slama, M. R. B., "Management strategies and root causes of missed iatrogenic intraoperative ureteral injuries with delayed diagnosis: a retrospective cohort study of 40 cases," *Patient Safety in Surgery* **17**(1), 21 (2023).

[4] Blackwell, R. H., Kirshenbaum, E. J., Shah, A. S., Kuo, P. C., Gupta, G. N., and Turk, T. M., "Complications of recognized and unrecognized iatrogenic ureteral injury at time of hysterectomy: a population based analysis," *The Journal of Urology* **199**(6), 1540–1545 (2018).

[5] Al-Taher, M., van den Bos, J., Schols, R. M., Bouvy, N. D., and Stassen, L. P., "Fluorescence ureteral visualization in human laparoscopic colorectal surgery using methylene blue," *Journal of Laparoendoscopic & Advanced Surgical Techniques* **26**(11), 870–875 (2016).

[6] Drake, M. and Noble, J., "Ureteric trauma in gynecologic surgery," *International Urogynecology Journal* **9**, 108–117 (1998).

[7] Vakili, B., Chesson, R. R., Kyle, B. L., Shobeiri, S. A., Echols, K. T., Gist, R., Zheng, Y. T., and Nolan, T. E., "The incidence of urinary tract injury during hysterectomy: a prospective analysis based on universal cystoscopy," *American Journal of Obstetrics and Gynecology* **192**(5), 1599–1604 (2005).

[8] Wiacek, A., Wang, K. C., and Bell, M. A. L., "Techniques to distinguish the ureter from the uterine artery in photoacoustic-guided hysterectomies," in [*Photons Plus Ultrasound: Imaging and Sensing*], **10878**, 478–484, SPIE (2019).

[9] Wiacek, A., Wang, K. C., Wu, H., and Bell, M. A. L., "Parking sensor-inspired approach to photoacoustic-guided hysterectomy demonstrated with human cadavers," in [*Photons Plus Ultrasound: Imaging and Sensing*], **11642**, 68–73, SPIE (2021).

[10] Wiacek, A., Wang, K. C., Wu, H., and Bell, M. A. L., "Photoacoustic-guided laparoscopic and open hysterectomy procedures demonstrated with human cadavers," *IEEE Transactions on Medical Imaging* **40**(12), 3279–3292 (2021).

[11] Allard, M., Shubert, J., and Bell, M. A. L., "Feasibility of photoacoustic-guided teleoperated hysterectomies," *Journal of Medical Imaging* **5**(2), 021213 (2018).

[12] Wiacek, A., Wang, K. C., Wu, H., and Bell, M. A. L., "Dual-wavelength photoacoustic imaging for guidance of hysterectomy procedures," in [*Advanced Biomedical and Clinical Diagnostic and Surgical Guidance Systems XVIII*], **11229**, 73–79, SPIE (2020).

[13] Lediju, M. A., Pihl, M. J., Dahl, J. J., and Trahey, G. E., "Quantitative assessment of the magnitude, impact and spatial extent of ultrasonic clutter," *Ultrasonic Imaging* **30**(3), 151–168 (2008).

[14] Lediju, M. A., Trahey, G. E., Byram, B. C., and Dahl, J. J., "Short-lag spatial coherence of backscattered echoes: Imaging characteristics," *IEEE Transactions on Ultrasonics, Ferroelectrics, and Frequency Control* **58**(7), 1377–1388 (2011).

[15] Graham, M. T. and Bell, M. A. L., "Photoacoustic spatial coherence theory and applications to coherence-based image contrast and resolution," *IEEE Transactions on Ultrasonics, Ferroelectrics, and Frequency Control* **67**(10), 2069–2084 (2020).

[16] Kempski, K. M., Wiacek, A., Graham, M., González, E., Goodson, B., Allman, D., Palmer, J., Hou, H., Beck, S., He, J., and Bell, M. A. L., "In vivo photoacoustic imaging of major blood vessels in the pancreas and liver during surgery," *Journal of Biomedical Optics* **24**(12), 121905–121905 (2019).

[17] Graham, M. T., Huang, J., Creighton, F. X., and Bell, M. A. L., "Simulations and human cadaver head studies to identify optimal acoustic receiver locations for minimally invasive photoacoustic-guided neurosurgery," *Photoacoustics* **19**, 100183 (2020).

[18] Bell, M. A. L., Ostrowski, A. K., Li, K., Kazanzides, P., and Boctor, E. M., "Localization of transcranial targets for photoacoustic-guided endonasal surgeries," *Photoacoustics* **3**(2), 78–87 (2015).

[19] Shubert, J. and Bell, M. A. L., "Photoacoustic imaging of a human vertebra: implications for guiding spinal fusion surgeries," *Physics in Medicine & Biology* **63**(14), 144001 (2018).

[20] González, E. A., Jain, A., and Bell, M. A. L., "Combined ultrasound and photoacoustic image guidance of spinal pedicle cannulation demonstrated with intact ex vivo specimens," *IEEE Transactions on Biomedical Engineering* **68**(8), 2479–2489 (2021).